Optical and electrical investigations of indium oxide thin films prepared by thermal oxidation of indium thin films

V. Damodara Das, Shahil Kirupavathy, Laxmikant Damodare, and N. Lakshminarayan

Citation: Journal of Applied Physics **79**, 8521 (1996); doi: 10.1063/1.362477
View online: http://dx.doi.org/10.1063/1.362477
View Table of Contents: http://scitation.aip.org/content/aip/journal/jap/79/11?ver=pdfcov
Published by the AIP Publishing

Optical and electrical investigations of indium oxide thin films prepared by thermal oxidation of indium thin films

V. Damodara Das,[a] Shahil Kirupavathy,[b] Laxmikant Damodare,[a] and N. Lakshminarayan[b]
Department of Physics, Thin Film Laboratory, Indian Institute of Technology, Madras, Madras 600 036, India

(Received 9 June 1995; accepted for publication 16 February 1996)

Indium oxide thin films have been prepared by thermal oxidation of vacuum-deposited indium thin films in air in an open furnace at about 600 K. These indium oxide thin films prepared by thermal oxidation have been examined for optical transparency by measuring their optical absorbance as a function of wavelength. From the optical absorption data, optical band gap and the nature of the forbidden energy gap in the indium oxide thin films have been determined. Electrical conductivity measurements have also been carried out on the above oxide films as a function of temperature during heating and cooling cycles in vacuum. It is found that after the first heating, electrical conductivity increases to a significant extent due to removal of point defect clusters due to annealing which contribute to both carrier generation and scattering. From the thermoelectric power measurements carried out, it has been concluded that electrons are the majority carriers in these indium oxide thin films. © *1996 American Institute of Physics.* [S0021-8979(96)06510-2]

I. INTRODUCTION

Transparent conducting oxide thin film coatings are important in solar cells, especially in photovoltaic devices which convert light into electrical energy. In solar cells, conducting oxide films are used as contact materials due to the fact that some of the transparent oxide films like indium oxide and indium tin oxide are not only transparent to visible light but also have very high electrical conductivity so that they can serve as good contact materials which also transmit light to pass on to the active layers of the solar cells. Several workers have investigated the properties of indium oxide films both regarding their optical transparency and good electrical conductivity. Most of the indium oxide and indium tin oxide films have been prepared by reactive deposition technique in a vacuum deposition unit.[1–7] The techniques adopted in reactive deposition of the films are reactive thermal evaporation, reactive sputtering using rf technique, reactive cosputtering technique, activated reactive evaporation technique, etc. In the present study, we have investigated the optical and electrical properties of indium oxide thin films prepared by a different technique—thermal oxidation of indium films vacuum-deposited on glass substrates.

II. EXPERIMENTAL TECHNIQUES

Indium films were deposited in a conventional vacuum deposition unit in a vacuum of better than 5×10^{-5} Torr on clean glass substrates held at room temperature. At a time a number of films were prepared in a single pump down and deposition. The glass substrates used for the film deposition were soda lime glass plates of size $2.5\times7.5\times0.2$ cm and were thoroughly cleaned. The cleaning procedure adopted was as follows: the films were kept in freshly prepared chromic acid overnight and then washed with distilled water. The glass plates were then kept in a detergent solution and cleaned using an ultrasonic cleaner. The glass plates were taken out of the soap solution and once again cleaned with distilled water. Finally, the glass plates were cleaned with acetone. The glass substrates for film deposition were kept symmetrically on a horizontal plane at a height of 25 cm above the evaporation source. The film deposition was made through masks of size 2.5×6.5 cm so that the lateral dimensions of the films formed were 2.5 cm and 6.5 cm. The evaporation source was a dimpled molybdenum boat which was resistively heated by passing a current of about 50 A through it. The indium films so formed were taken four at a time for thermal oxidation in air in an open muffle furnace which could be heated to 600 K at which temperature it was known from the earlier work[8] that indium films get completely oxidized. After the oxidation was complete, it was ascertained by x-ray diffractometry that the indium films were completely oxidized at this temperature in the one hour duration for which the indium films were heated in air. The oxide films were investigated for optical transparency by optical absorption measurements and electrical conduction behavior by measuring their electrical resistance during cycles of heating and cooling in a vacuum of the order of 5×10^{-5} Torr. Thermoelectric power measurements were also made (in vacuum) to determine the type of carriers responsible for conduction in the indium oxide films. Optical absorption studies were carried out in the Hitachi recording spectrophotometer (model U 3400 with range 190 nm to 2500 nm, and resolution 2 nm) in the optical region, viz. between 300 nm and 900 nm. The optical absorption spectrum in the glass substrate was also taken and it was used for the elimination of optical absorption in the glass plates from the total absorption in the film-substrate combination to get the optical absorption in the films.

[a]Electronic mail: phy10@iitm.ernet.in
[b]Also at Madras Christian College, Tambaram, Madras 600 059, India.

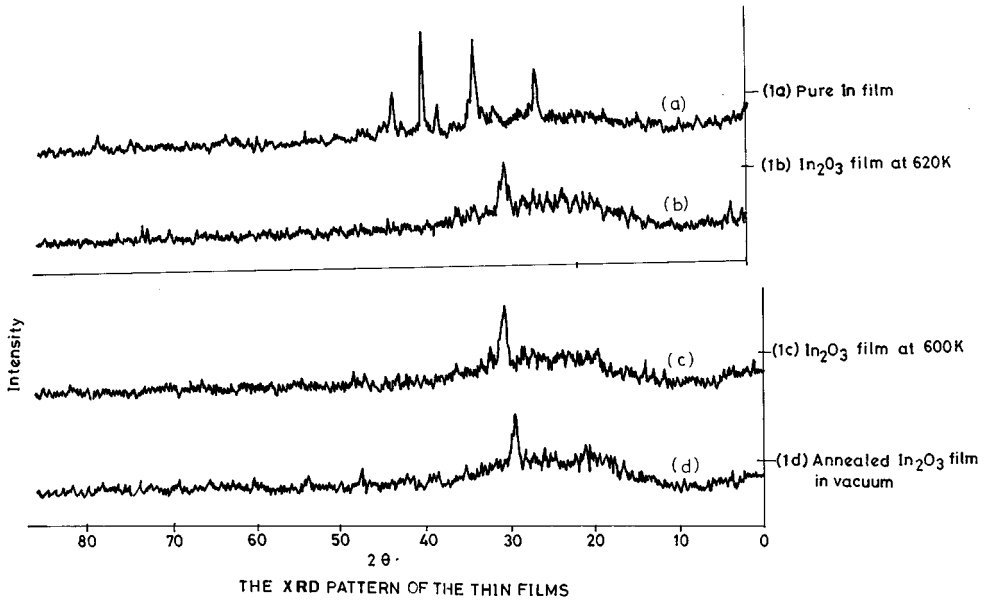

FIG. 1. X-ray diffractograms of (a) the as-deposited indium film, (b) after oxidation at 600 K in air for 1 h, (c) after postoxidation annealing in air for 1 h at 600 K, (d) after postannealing for 1 h in vacuum.

III. RESULTS AND DISCUSSION

A. Structural characterization

1. X-ray diffraction studies

Figures 1(a)–(d) show the x-ray diffractograms of (a) the as-deposited indium film, (b) after oxidation at 600 K in air for 1 h, (c) after postoxidation annealing in air for 1 h at 600 K, and (d) after postoxidation annealing for 1 h, in vacuum. It is seen that Fig. 1(a) contains a few characteristic x-ray diffraction peaks of indium while Figs. 1(b)–(c) all contain only one prominent peak and other shallow diffraction peaks of low intensity which are characteristic of In_2O_3. It should be mentioned that postoxidation annealing either in air or in vacuum did not change the intensities of the shallow peaks. Figures 2(a) and 2(b) show typical x-ray diffractograms of thicker films oxidized at 600 K in air. It is seen from these figures that the shallow peaks in x-ray diffractograms in Figs. 1(b)–(d) have become a little more prominent in the case of thicker films. In Tables I and II, the d values calculated are tabulated from the positions of the diffraction peaks in Figs. 1 and 2. In the above tables, these d values are also compared with the standard d values of indium and indium oxide as reported in American Society for Testing Materials (ASTM) cards numbers 5–642 and 21–406, respectively. It can be seen from Figs. 1 and 2 and Tables I and II that as-deposited indium films are pure indium films and after oxidation, we do not have any traces of indium and the films are completely of indium oxide.

2. Electron microscopic studies

Electron microscopic studies were also made on as-deposited indium thin films and the indium oxide films

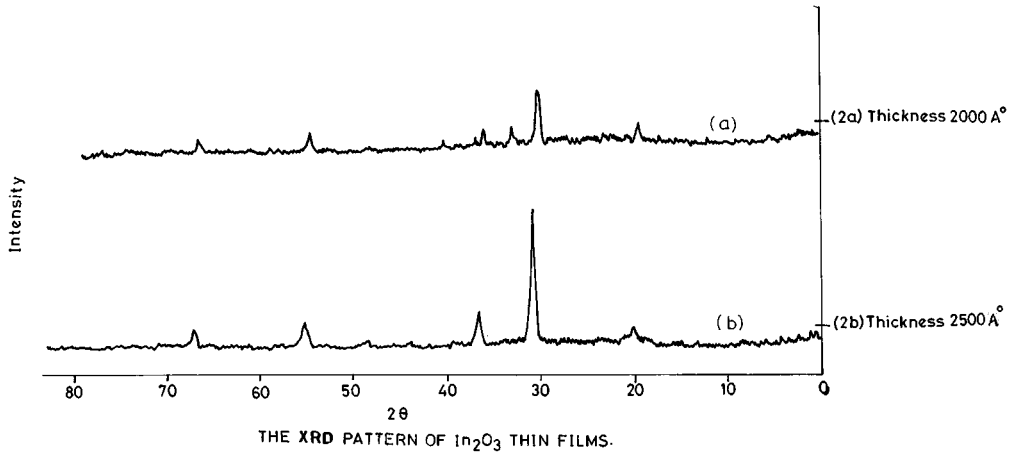

FIG. 2. (a) and (b) Typical x-ray diffractograms of thicker films oxidized at 600 K in air.

TABLE I. d values corresponding to Fig. 1(a) (indium film). Standard d values of indium from ASTM Card No. 5–642 (structure: tetragonal).

Sl. No.	Observed d from XRD (Å)	Standard d (Å)	h	k	l
	(a)				
1	2.6832	2.715	1	0	1
2	2.4134	2.471	0	0	2
3	2.3268	2.298	1	1	0

formed after oxidation of these films in air. Figures 3(a) and 3(b) show the typical electron micrograph and selected area electron diffraction pattern of as-deposited indium films while Figs. 4(a) and 4(b) show the typical micrograph and the diffraction pattern in the case of indium oxide thin films. It is seen that there is a lot of background intensity due to diffuse scattering in the case of indium films similar to amorphous materials but the micrograph shows that there are well developed microcrystallites in the film and the d values calculated from the diffraction pattern match fairly well with the standard d values of indium (Table III). Table IV shows the d values calculated from the diffraction pattern in Fig. 4(b) which are compared with the standard d values of indium oxide. It is seen that there is very good agreement of d values with the standard ones. Thus, both the x-ray diffractograms and electron microscopy work show that the films formed after thermal oxidation in air of indium films are indium oxide films and there are no traces of indium which can be detected by either x-ray diffraction or electron diffraction. It can also be seen that there is a symmetrically located hexagonal network of sharp spots in the electron diffraction ring pattern of indium oxide films from which we can conclude that there is a tendency for the films to have their microcrystallites preferentially oriented with their ((111)) planes parallel to the substrate on which they are grown. This fact is also evident from the x-ray diffractograms from which it is seen that the diffraction peak corresponding to ((111)) set of planes is many times more prominent than the other diffraction peaks.

TABLE II. (a) d values corresponding to Fig. 2(a) (In_2O_3 film 2000 Å). Standard d values of In_2O_3 from ASTM Card No. 21–406 (structure: cubic). (b) d values corresponding to Fig. 2(b) (In_2O_3 film 2500 Å). Standard d values of In_2O_3 from ASTM Card No. 21-406 (structure: cubic).

Sl. No.	Observed d from XRD (Å)	Standard d (Å)	h	k	l
	(a)				
1	4.1444	4.130	2	1	1
2	2.9281	2.921	2	2	2
3	2.7233	2.704	3	2	1
4	2.5312	2.529	4	0	0
5	1.7919	1.788	4	4	0
6	1.5258	1.525	6	2	2
	(b)				
1	4.1410	4.130	2	1	1
2	2.9253	2.921	2	2	2
3	2.5344	2.529	4	0	0
4	1.7903	1.788	4	4	0
5	1.5278	1.525	6	2	2

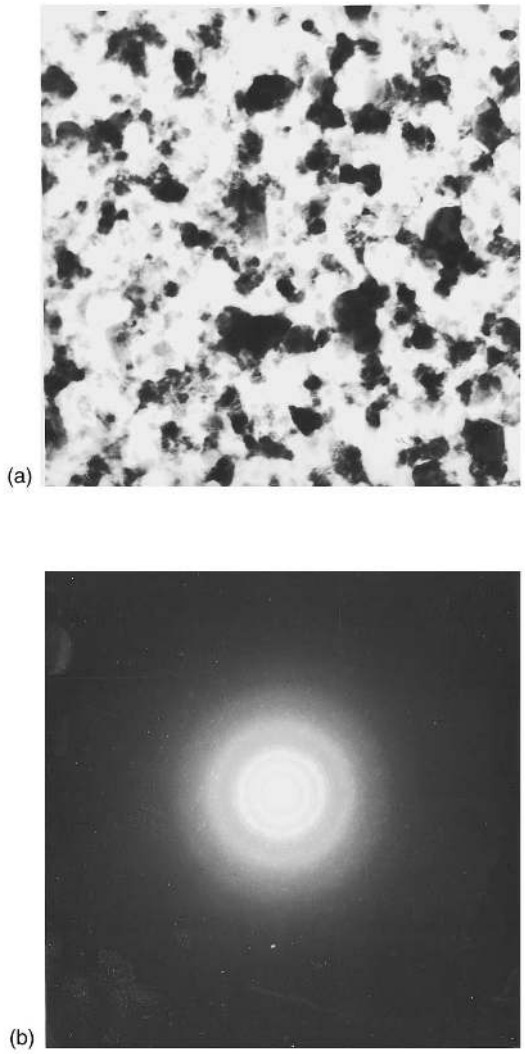

FIG. 3. (a) and (b) typical electron micrograph and selected are diffraction pattern of as-deposited indium films.

3. Energy dispersive analysis of x rays

Energy dispersive analysis of x rays (EDAX) generated by the incident electron beam on indium and indium oxide films was also carried out to investigate the stoichiometry of the indium oxide films formed. Figures 5(a) and 5(b) show the EDAX spectra of indium film and indium oxide film. Table V and Table VI give the composition results of EDAX spectra of indium film and indium oxide film. It is seen from Fig. 5 that the as-deposited indium film consists of 100% pure indium while the indium oxide film consists of 61.8 atomic % indium and 38.2 at. % oxygen which deviates a little from stoichiometry of 60% indium and 40% oxygen of In_2O_3. There is about 3% oxygen deficiency. However, the stoichiometry of the indium oxide films formed varies somewhat (about 5%) up to a maximum of about 10% from one specimen to the other.

B. Optical absorption studies

The In_2O_3 films formed by thermal oxidation as described before were investigated for optical absorption in the

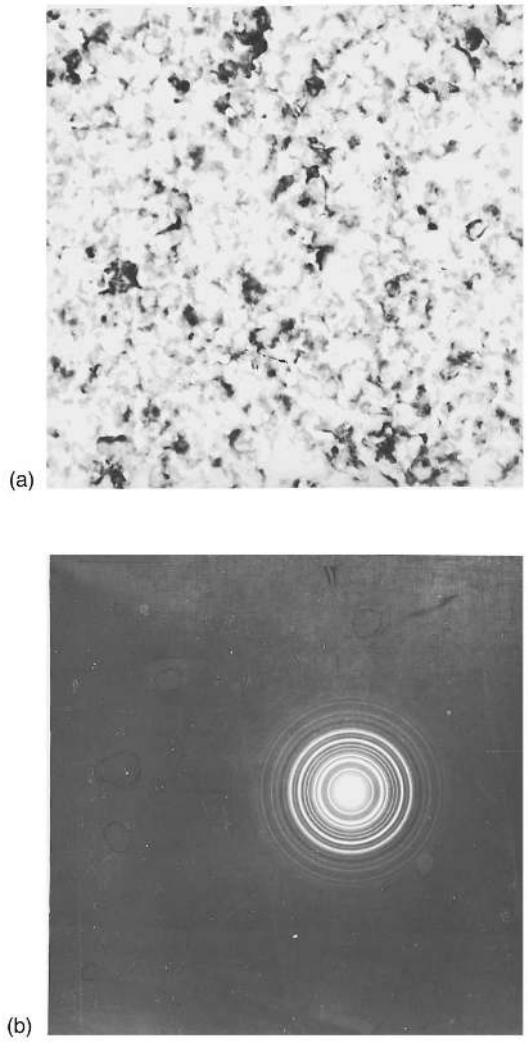

FIG. 4. (a) and (b) typical micrograph and the diffraction pattern in the case of indium oxide films.

optical region using a Hitachi recording spectrophotometer (Model U3400). As the films were examined along with the glass substrate on which they were formed, it is necessary to take into account the absorption in the glass substrate on which they were formed even though it is small. Hence, the absorption spectrum of the glass plate was also taken. Figure 6 shows the optical transmission vs wavelength for a few typical films of different thicknesses (1700 Å, 2200 Å, 3250 Å, respectively) in the optical region (200–850 nm). It is seen from the plots that the thicker films of thickness 3250 Å are more transparent with about 90–95% transmission in the

TABLE III. *d* values corresponding to Fig. 4(a) (indium). Standard *d* values of indium from ASTM Card No. 5–642 (structure: tetragonal).

Sl. No.	Observed *d* from electron diffraction (Å)	Standard *d* (Å)	*h*	*k*	*l* (Å)
1	2.9312	2.715	1	0	1
2	2.5912	2.4715	0	0	2
3	1.4175	1.470	1	0	3

TABLE IV. *d* values corresponding to Fig. 4(b) (In_2O_3 film). Standard *d* values of In_2O_3 from ASTM Card No. 21–406 (structure: cubic).

Sl. No.	Observed *d* from XRD (Å)	Standard *d* (Å)	*h*	*k*	*l*
1	2.8862	2.921	2	2	2
2	2.7164	2.704	3	2	1
3	1.8456	1.848	5	2	1
4	1.4371	1.431	5	4	3
5	1.2896	1.285	7	3	2
6	1.0734	1.0786	6	6	4

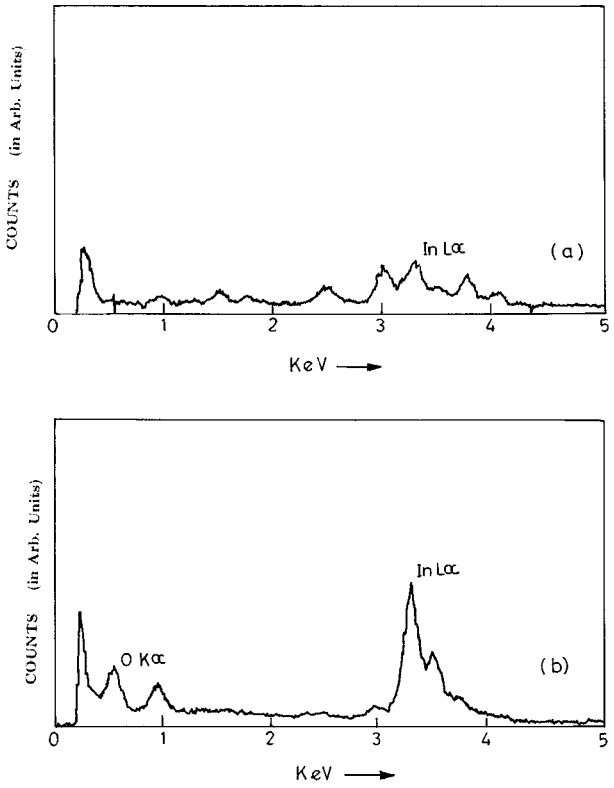

FIG. 5. (a) and (b) EDAX spectra of indium film and indium oxide film.

TABLE V. EDAX compositional analysis data from Fig. 5(a).

Sl. No.	Element	At. % element
1	In L	100

TABLE VI. EDAX compositional analysis data from Fig. 5(b).

Sl. No.	element	At. % element
1	O K	61.797
2	In L	38.203

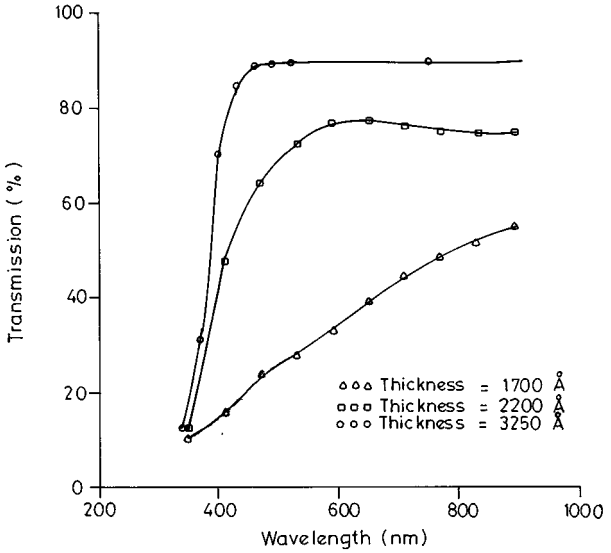

FIG. 6. Plots of optical transmission vs wavelength for various thicknesses.

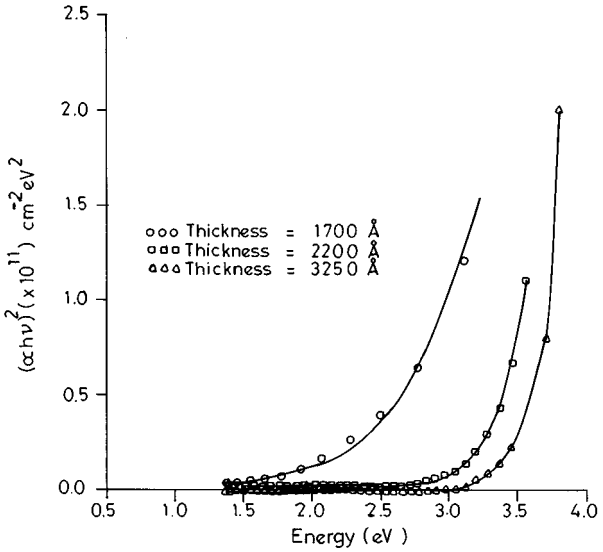

FIG. 7. Plots of $[\alpha h\nu]^2$ vs $h\nu$ for various thicknesses.

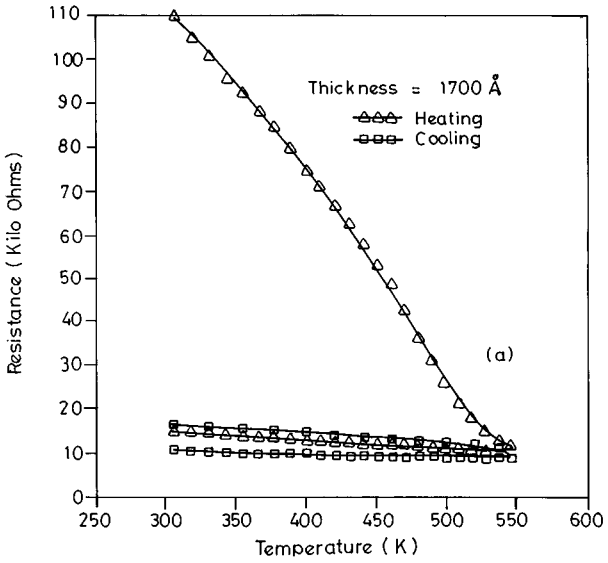

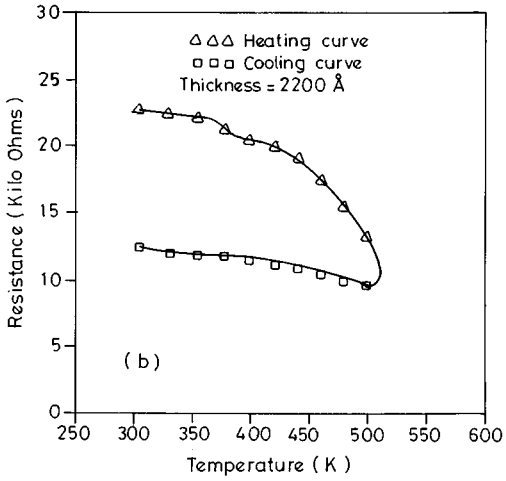

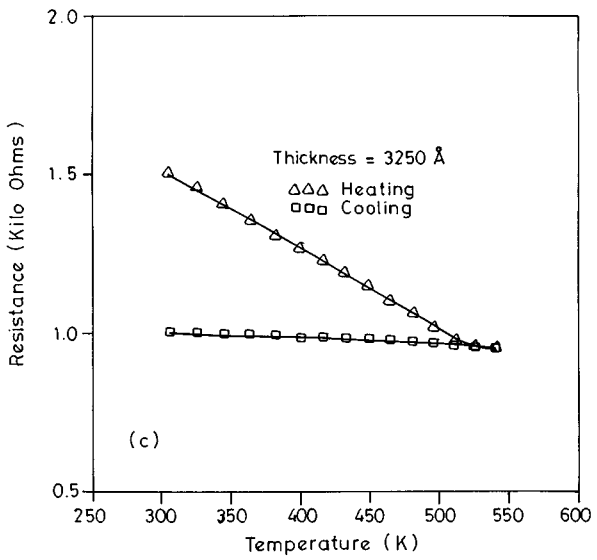

FIG. 8. (a)–(c) Variation of electrical resistance as a function of temperature during heating–cooling cycles for In_2O_3 films of thicknesses 1700 Å, 2200 Å, 3250 Å, respectively.

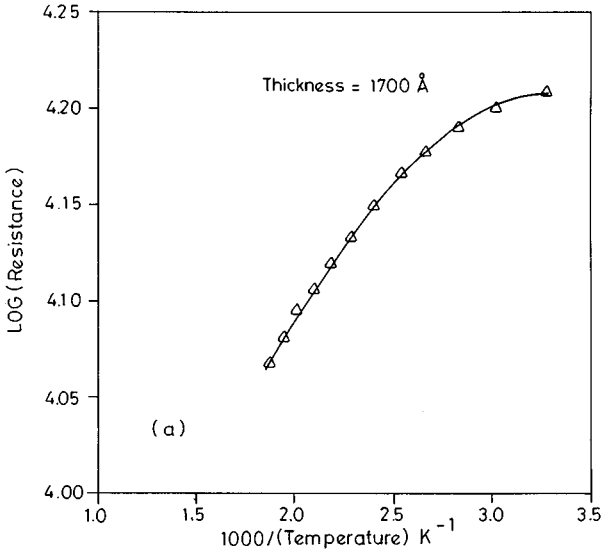

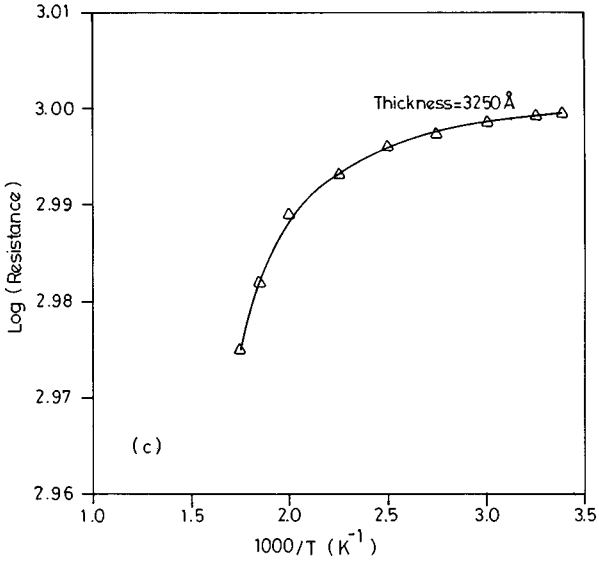

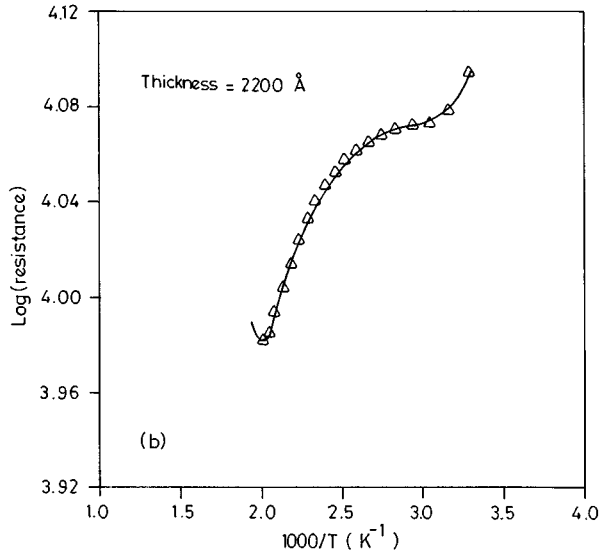

FIG. 9. Plots of log (resistance) vs reciprocal of temperature for thicknesses 1700 Å, 2200 Å, 3250 Å, respectively.

visible region (400–750 nm) whereas the films of thickness of 2200 Å are transparent with transmission of about 75–85% in the visible region (400–750 nm). The films of thickness of about 1700 Å are less transparent with transmission of about 30–50% in the visible region (400–750 nm). Thus, it can be concluded that the thicker films are better suited for devices due to their high transparency.

From the transmission data, the absorption coefficient as a function of photon energy was calculated and was plotted for the direct allowed transition by using the formula,

$$[\alpha] \approx \left[\frac{A}{h\nu}\right][h\nu - E_g]^{1/2},$$

where E_g is the transition energy gap and $h\nu$ is the photon energy. Figure 7 shows the $[\alpha h\nu]^2$ vs $h\nu$ plots for various thicknesses. The direct band gap value is obtained for the films with thickness of about 3250 Å as 3.5 eV which is close to the values quoted in the literature.[10,11]

From Fig. 7, the plots of $(\alpha h\nu)^2$ vs $h\nu$ indicate that there is some amount of tailing in the band gap below the absorption edge. This indicates that there is a high concentration of impurity states in polycrystalline indium oxide films which can cause a perturbation of the band structure with the result that the parabolic distribution of the states will be disturbed by a prolonged tail extending into the energy gap.[12]

The tails in optical absorption spectra of indium oxide can be due to the following:

(i) The broadening of the impurity levels due to their spatial overlap into a band. At high concentrations, the impurity band merges with the nearest intrinsic band. Due to this, the Fermi level will lie inside the parabolic portion of the appropriate band, which in our case is the conduction band.

(ii) The impurities which can be ionized donors exert an attractive force on the conduction electrons and a repulsive force on the valence band. On a microscopic level, the nonhomogeneous distribution of the impurities leads to smearing of the band edges.[13]

C. Electrical conductivity studies

The electrical conductivity of In_2O_3 films was measured in a vacuum of 5×10^{-5} Torr during one or two cycles of heating and cooling for films of different thicknesses. Figures 8(a)–(c) show the variation of electrical resistance as a function of temperature during heating–cooling cycles for In_2O_3 films of thicknesses 1700 Å, 2200 Å, and 3250 Å, respectively. It is seen from Fig. 8(a) that during the first heating cycle, the resistance of the film sharply decreases monotonically with increase in temperature. During the first cooling cycle the resistance increases with the decrease in temperature, but the increase in resistance is only moderate when compared to the resistance change during the first heating cycle. During the second heating cycle also resistance falls with the increase in temperature but the resistance change is again moderate with the second heating cycle curve closely following the first cycle cooling curve. During the second cycle cooling, the resistance variation with temperature is nearly the same as that during the first cycle cooling. Figures 8(b) and 8(c) also show similar resistance variation with temperature during heating and cooling where the variation for only one cycle of heating and cooling is plotted. Even though the decrease in resistance with increase in temperature during the first heating is much smaller compared to that of the thinner film in Fig. 8(a), the decrease is much larger than the change in the first cycle cooling. It is seen from the plots that in the case of all the curves, during the first cycle of heating there is a sharp decrease of resistance as a function of temperature, whereas during the subsequent heating and cooling cycles, the resistance variation with temperature is small. The steep fall in resistance with increase in temperature during the first heating can be explained by two

TABLE VII. Activation energy from conductivity measurements.

Sl. No.	Thickness of the film (Å)	Activation energy (meV)
1	1700	14.17
2	2200	12.52
3	3250	11.59

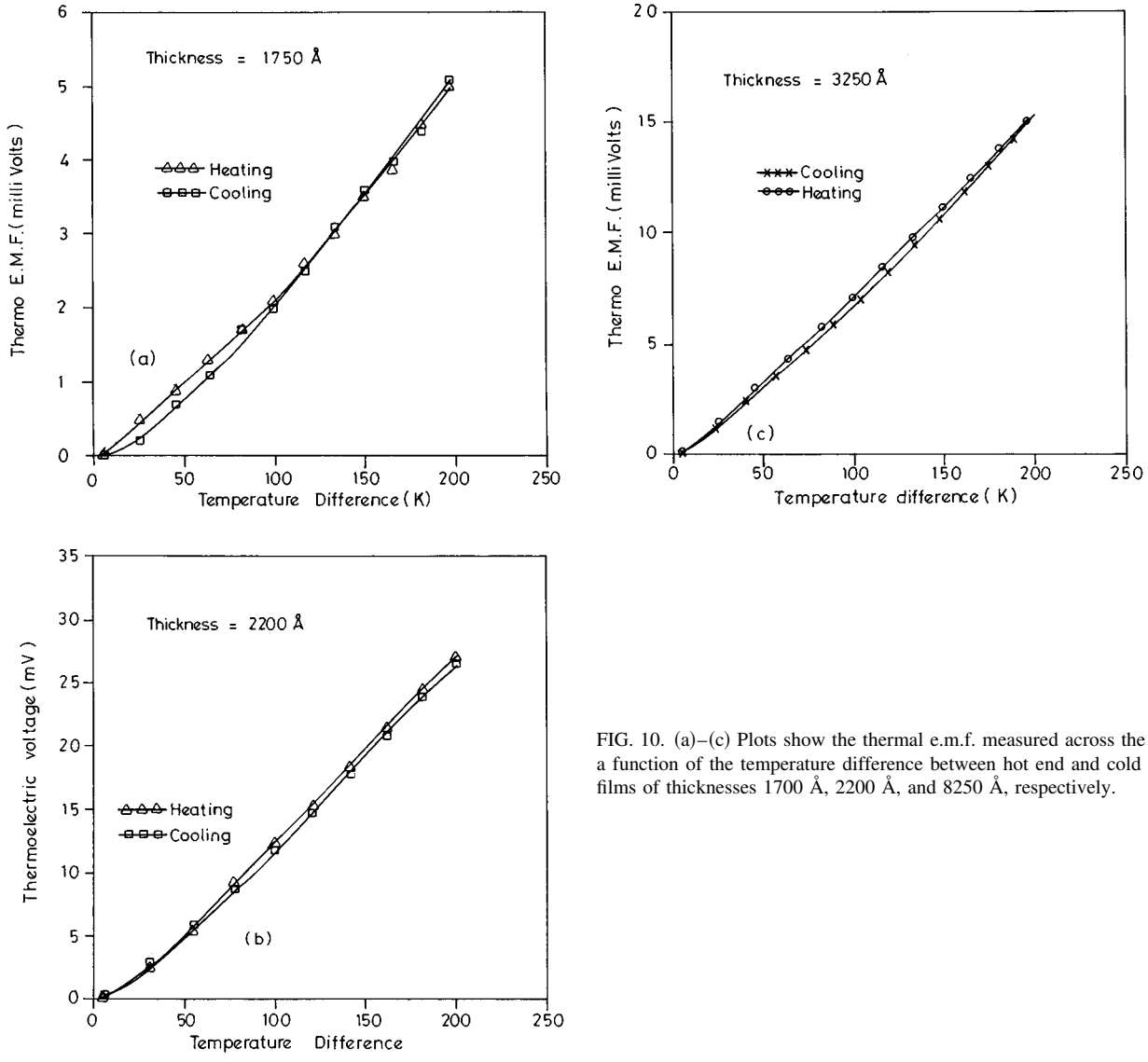

FIG. 10. (a)–(c) Plots show the thermal e.m.f. measured across the film as a function of the temperature difference between hot end and cold end for films of thicknesses 1700 Å, 2200 Å, and 8250 Å, respectively.

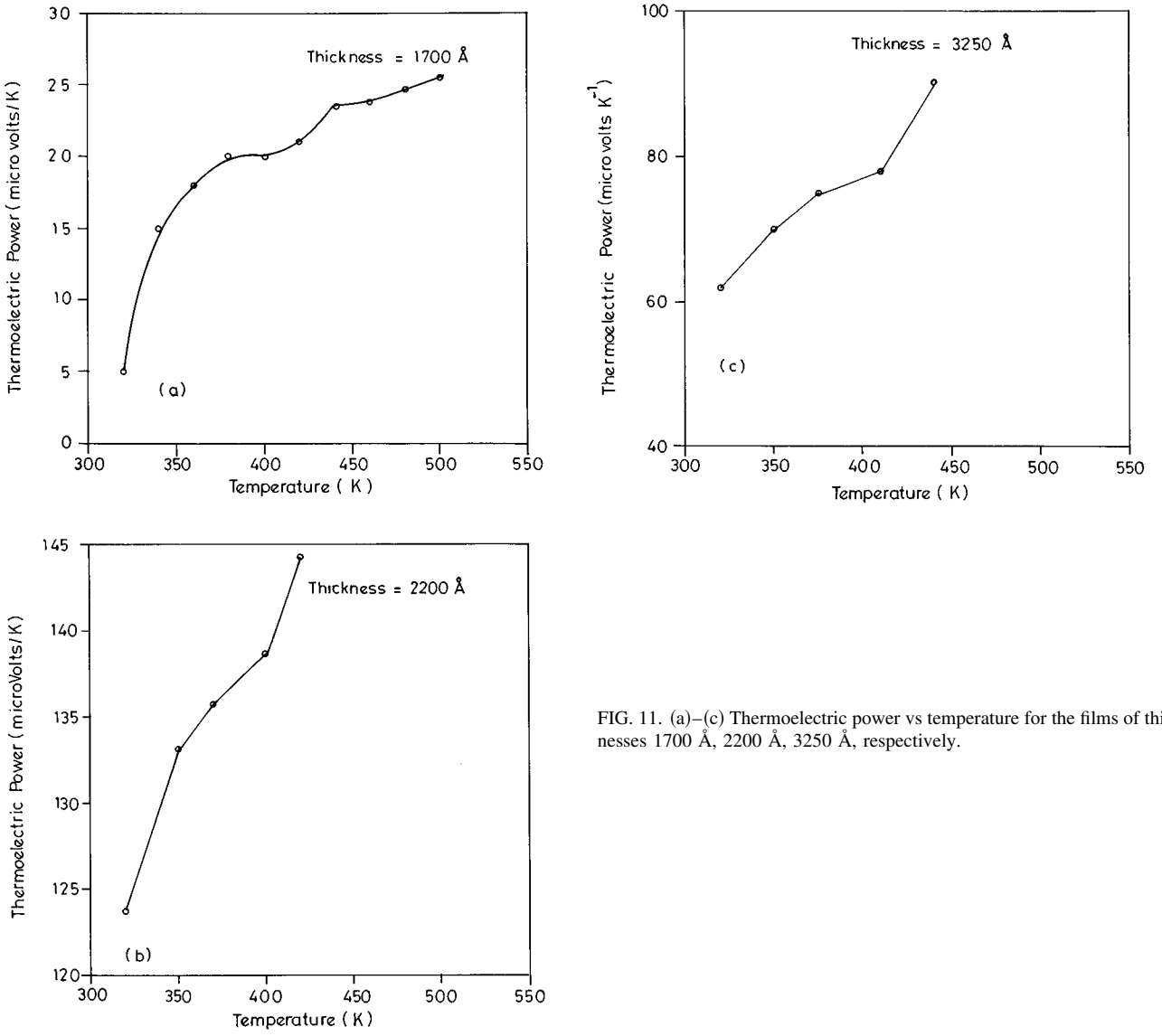

FIG. 11. (a)–(c) Thermoelectric power vs temperature for the films of thicknesses 1700 Å, 2200 Å, 3250 Å, respectively.

mechanisms. First, any point defects of a combined type, i.e., point defect clusters, present in the In_2O_3 films get rearranged and removed by small scale diffusion, thereby causing a decrease in carrier scattering by these point defect clusters. Consequently, the resistance,[14–22] can decrease. The removal of point defect cluster defects on annealing of the films is well known. Many theories have been developed to explain defect removal during annealing.[14–17] Second, because of the rearrangement of the point defect clusters and their removal in which oxygen plays an important role since the lattice of In_3O_3 contains indium and oxygen point defects. Thus, rearrangement and elimination of point defect clusters leads also to an increase in the carrier concentration, thereby decreasing the electrical resistance. It is also seen from the figures that after annealing, the resistance of the films is very low, of the order of a few kΩ or less at room temperature, depending upon the film thickness. As a matter of fact, the film of thickness 3250 Å has a resistance of only 1 kΩ at room temperature which decreases marginally with increase in temperature. This amounts to an electrical conductivity of 125×10^2 $(\Omega\,\mathrm{cm})^{-1}$. Thus, these films can find application as good transparent conducting coatings. From the first cycle cooling data, log (resistance) vs reciprocal temperature plots were drawn as shown in Figs. 9(a)–9(c) for the films of thicknesses 1700 Å, 2200 Å, and 3250 Å. It is seen that the plots are nearly linear in the high temperature region above about 400 K. The activation energy for conduction calculated from the slopes of these plots are tabulated in Table VII.

D. Thermoelectric power studies

Thermoelectric power of the above films was also determined as a function of temperature in a vacuum better than 5×10^{-5} Torr using the integral method in which one end of the film is heated by a mini heater. The other end of the film is clamped to a massive copper block in contact with the base plate of the vacuum deposition unit so that it is in good thermal contact. Thus, the film end connected to this copper block remains essentially at the ambient temperature. Rise in

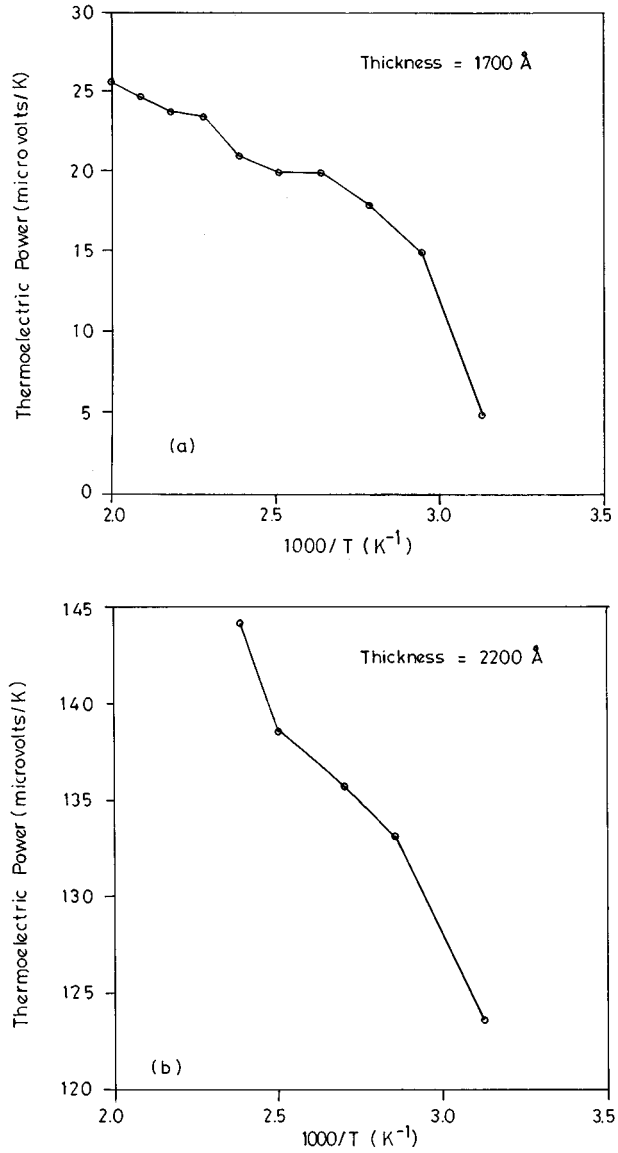

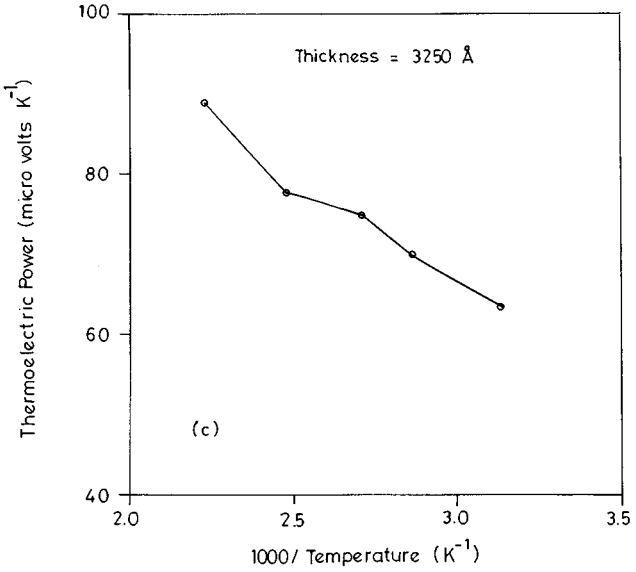

FIG. 12. (a)–(c) Plot of variation of thermoelectric power with reciprocal of temperature.

temperature of this end was less than 1° during the measurement. The thermal e.m.f. was measured with reference to copper and temperatures of cold and hot ends were recorded using copper constantan thermocouples which were clamped right on the film. Figures 10(a)–10(c) show the thermal e.m.f. measured across the film as a function of the temperature difference between the hot end and the cold end for similar films of thicknesses 1700 Å, 2200 Å, and 3250 Å during one or two cycles of heating and cooling. It is seen from the figures that the thermal e.m.f.s developed increase with an increase in temperature differences for all the three films and the thermal e.m.f. developed during heating and cooling for a given temperature difference are very nearly the same during one or two cycles of heating and cooling. From the above plots of thermal e.m.f. vs temperature difference, thermoelectric power was calculated as slopes of the above curves at different temperatures. For the determination of the thermoelectric power, only the first cycle cooling curve was taken. Figures 11(a)–(c) show the thermoelectric power vs temperature for the above films determined as described above. It is seen from the figures that the thermoelectric power increases linearly with an increase in temperature in the case of all the films. It is seen from the figures that at a given temperature (say 400 K) it is 20 μV/K, 140 μV/K and 80 μV/K, respectively, in the three cases. Thus, even though the thermoelectric power depends on thickness of the films it does not appear to depend upon the film thickness uniformly. The thermoelectric power was also plotted as a function of reciprocal temperature to investigate the conducting state of the material. It is found from Figs. 12(a)–(c) that the material is a semiconductor as thermoelectric power vs reciprocal temperature plots are near linear, which agrees with the equation for a n-type nondegenerate semiconductor:

$$S = -\left(\frac{k_B}{e}\right)\left[A + \frac{E_0}{k_B T}\right], \tag{1}$$

where S is the thermoelectric power; k_B is the Boltzmann constant; E_0 is the activation energy; A is the scattering parameter, and e is the charge on the electron. From the slopes

TABLE VIII. Activation energy from thermoelectric power measurements.

Sl. No.	Thickness of the film (Å)	Activation energy (meV)
1	1700	14.9
2	2200	25.42
3	3250	26.68

of the plots, the activation energy was calculated and is tabulated in Table VIII for different film thicknesses. It was found that the hot end of the film was positive and hence the majority carriers in the In_2O_3 films are electrons because the hot end being positive indicates that the electrons have drifted away from the hot end towards the cold end of the film thereby making the hot end of the film positive. Thus, the present In_2O_3 films exhibit n-type conduction and the majority carriers are electrons.

IV. CONCLUSIONS

It is concluded from the above study that the indium oxide thin films prepared by thermal oxidation in air of vacuum-deposited indium thin films on glass substrates have good transparency, thicker films having transmission of about 90–95% or more in the entire visible region. It is also found that the electrical conductivity of the thicker films is more than 125×10^2 $(\Omega\,\mathrm{cm})^{-1}$. It is further found that electrons are the majority carriers in these indium oxide thin films and the films are all, therefore, n type. It is also concluded that the thermoelectric power of the films is thickness dependent.

[1] J. R. Bosnell and R. Waghorne, Thin Solid Films **15**, 141 (1973).
[2] H. W. Lehmann and Widmer, Thin Solid Films **27**, 359 (1975).
[3] S. Ohhata, F. Shinoki, and S. Yoshida, Thin Solid Films **59**, 255 (1979).
[4] P. Nath and R. F. Bunshah, Thin Solid Films **69**, 63 (1980).
[5] M. Mizuhashi, Thin Solid Films **70**, 91 (1980).
[6] O. Marcovitch, Z. Klein, and I. Lubezky, Appl. Optics **28**, 2792 (1989).
[7] H. Shmuelli and R. Rosenbaum, Physica B **169**, 489 (1992).
[8] V. Damodara Das and D. Subbu, 8th International Conference Thin Films and 17th International Conference on Metallic Coatings, San Diego, CA, April 1–6, 1990.
[9] K. L. Chopra and S. R. Das, *Thin Film Solar Cells* (Plenum, New York), pp. 321–328.
[10] H. K. Muller, Phys. Status Solidi **27**, 723 (1968).
[11] R. L. Weiher and R. P. Lev, J. Appl. Phys. **37**, 299 (1966).
[12] R. H. Parmenter, Phys. Rev. **97**, 587 (1955).
[13] J. I. Pankove, Phys. Rev. A **140**, 2059 (1965).
[14] V. Vand, Proc. Phys. Soc. **55**, 222 (1943).
[15] W. Primak, Phys. Rev. **100**, 1677 (1955).
[16] C. J. Meechan and J. A. Brinkman, Phys. Rev. **103**, 1193 (1956).
[17] V. Damodara Das, J. Appl. Phys. **55**, 1023 (1984).
[18] V. Damodara Das and M. S. Jagadesh, Thin Solid Films **24**, 203 (1974).
[19] K. Narayanadas, M. R. Adhakrishnan, and C. Balasubramanian, Thin Solid Films **67**, 357 (1980).
[20] P. G. Wilkinson, J. Appl. Phys. **22**, 419 (1951).
[21] V. V. Shah and Y. G. Naik, Indian J. Pure Appl. Phys. **2**, 20 (1965).
[22] H. Toyoda and M. Nagashima, J. Phys. Soc. Jpn. **14**, 274 (1959); Proc. Phys. Soc. **55**, 222 (1943).